

Vibrational Bandstructures of Bottom-Up Built Nanoscale Phononic Crystals

R. Meyer*

*Department of Mathematics and Computer Science and Department of Physics,
Laurentian University, 935 Ramsey Lake Road, Sudbury (Ontario) P3E 2C6, Canada*

(Dated: November 2, 2015)

The vibrational properties of a phononic crystal assembled from Si nanoparticles and nanowires is studied with large-scale molecular-dynamics simulations. The phonon dispersion relations derived from the simulations show the existence of acoustic band gaps in the bottom-up built phononic crystal. Further insight into the nature of the vibrational modes is obtained with the help of a finite element analysis of a simple two-dimensional model. The vibrational modes of this model demonstrate how the phononic crystal moves away from plane wave behavior at shorter wavelengths. At wavelengths comparable to the structure size of the phononic crystal, modes form that decouple the vibrations of nanoparticles and nanowires.

PACS numbers: 63.22.-m, 02.70.Ns

Phononic crystals (PnCs) are periodically structured synthetic materials that use Bragg reflection to manipulate the propagation of phonons. Recently, these materials have received increasing scientific attention due to a wide range of potential technological applications. PnCs are expected to have a significant impact on areas ranging from ultrasonic imaging and noise control to wireless communications and thermal management [1, 2].

Nanofabrication methods make it possible to synthesize hypersonic PnCs with periodicity length in the sub-micron range and operating frequencies in the GHz - THz range [3]. In this work, the vibrational properties of a nanoscale PnC built from Si nanowires and nanoparticles are studied. This bottom-up approach is different from the top-down approach employed in most studies of nanoscale PnCs (see e.g. [3–7]) where a periodic arrangement of scatterers (voids or inclusions) is embedded into a matrix. In the system studied in this work, the nanoparticles act as scatterers that are not embedded into a matrix but connected by the nanowires. The results show that this technique is able to produce materials with acoustic band-gaps. In addition to potential technological applications, these structures are fundamentally interesting as they are a transition between a continuum and a system of interacting particles.

Molecular-dynamics (MD) simulations is an important tool for the modelling of nanoscale systems. For systems with structure sizes in the nm range, macroscopic scaling laws and continuum theories reach their limits and the atomic nature of the underlying material makes itself felt. In the case of nanoscale PnCs, deviations from linear elasticity theory were first shown by Ramprasad and Shi [8]. As an atomistic method, MD is able to describe the typical effects of the nanoscale.

The system simulated in this work is shown in Fig. 1. It was built by placing 240 spherical Si nanoparticles with diameters of 7.5 nm and 9.9 nm on the sites of a binary honeycomb lattice ($a = 28.87$ nm). The particles were then connected by cylindrical nanowires with a diameter

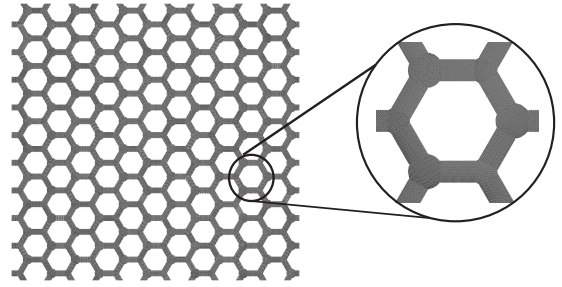


FIG. 1. View of the configuration used in the MD simulations

of 6 nm. The wires followed the (001) direction of the Si lattice. In order to enhance the realism of the simulation, all nanoparticles and nanowires were randomly rotated, so that grain boundaries were created at the interfaces between particles and wires. The system contains 9,009,688 Si atoms and covers an area of $299 \text{ nm} \times 288 \text{ nm}$.

The MD simulations of the system employed a modified embedded atom method potential for Si [9]. Although this potential exaggerates the higher phonon frequencies [10, 11], it gives a good qualitative description of the phonon spectrum and elastic properties which is sufficient for the goals of this work. The simulations used the velocity-form of the Verlet algorithm with a time step $\Delta t = 1$ fs. Simulations of systems of this size require the use of parallel computers. Normal domain decomposition, however, has load balancing problems for strongly inhomogeneous systems like the PnC simulated in this work. Therefore the method described in Ref. [12] was employed to achieve a high parallel efficiency.

The vibrational properties of the model system were derived with the help of the velocity-autocorrelation function (VACF). The total vibrational density of states (VDOS) $g(\nu)$ is proportional to the Fourier transform of the VACF averaged over all atoms:

$$g(\nu) = \int_{-\infty}^{\infty} dt \frac{\sum_{i=1}^N \langle \mathbf{v}_i(t) | \mathbf{v}_i(0) \rangle}{\sum_{i=1}^N \langle \mathbf{v}_i(0) | \mathbf{v}_i(0) \rangle} e^{i2\pi\nu t} \quad (1)$$

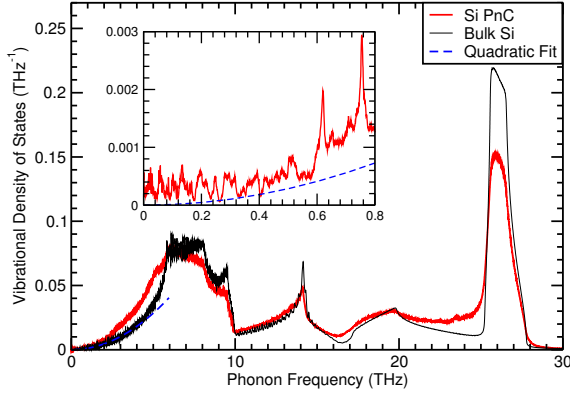


FIG. 2. (Color online) Normalized VDOS of the simulated PnC compared to bulk Si. The blue line represents a quadratic fit of the low frequency part ($0.5\text{THz} < \nu < 4\text{THz}$) of the bulk system.

For periodic systems, frequencies of individual modes can be derived by projecting the velocities onto a plane wave with wave vector \mathbf{q} and polarization direction \mathbf{p}

$$\hat{v}_{\mathbf{q}}^{\mathbf{p}}(t) = \sum_{i=1}^N \mathbf{p} \cdot \mathbf{v}_i(t) e^{-i\mathbf{q} \cdot \mathbf{r}_i^0} \quad (2)$$

(where \mathbf{r}_i^0 denotes the equilibrium position of atom i) and calculating the VACF of the projected velocity [11, 13]:

$$g_{\mathbf{q}}^{\mathbf{p}}(\nu) = \int_{-\infty}^{\infty} dt \frac{\langle \hat{v}_{\mathbf{q}}^{\mathbf{p}}(t) | \hat{v}_{\mathbf{q}}^{\mathbf{p}}(0) \rangle}{\langle \hat{v}_{\mathbf{q}}^{\mathbf{p}}(0) | \hat{v}_{\mathbf{q}}^{\mathbf{p}}(0) \rangle} e^{i2\pi\nu t} \quad (3)$$

For the derivation of the vibrational properties of the PnC system from the VACF the size of the data set leads to technical problems. To cover the full spectrum of the system it was necessary to use the velocity data over a period of more than 1 ns at intervals of not more than 15 fs. For a system with more than 9 million atoms, this gives more than 12 TB of data. In addition to the storage problem, it would be challenging to process this amount of data. This problem was overcome by selecting a random subset of 250,000 atoms and using only these atoms in the summations of Eq. 1 and 2. This sampling method can be interpreted as an analogue to a Monte-Carlo integration where the integration over all space is replaced by the summation of a large enough random sample.

To derive the velocity data for the VACF calculations, the system was first thoroughly equilibrated. Then the velocity data of the random subset were stored during a simulation at intervals of 15 fs until $2^{17} = 131072$ time samples of the velocities covering a period of 1.966 ns had been collected. The size of this data set is "only" 366 GB.

Fig. 2 compares the total VDOS obtained for the PnC system to the VDOS of a bulk Si system. To reduce the remaining noise, the data of the PnC (bulk) system have been broadened by a finite line-width of 1 GHz (5 GHz). The main part of the figure shows that at high frequencies

the VDOS of the PnC system has a structure similar to that of the bulk system. The height of the peak, however, is severely reduced and the VDOS of the PnC system is generally higher on the left flanks of the peaks indicating a shift to lower frequencies. This behavior is similar to the results reported in Ref. [11] where it was shown that these changes are caused by surface modes.

The inset of Fig. 2 shows the low frequency part of the total VDOS of the PnC system. A direct comparison to simulations of a bulk system is not possible since it would require simulations of a much larger bulk system. Since the VDOS of an infinite bulk system scales as ν^2 at low frequencies, we extrapolate the bulk data with the help of a quadratic fit. The inset shows that the VDOS of the PnC system has a lot of structure at low frequencies which gives evidence of the modification of the VDOS due to the periodic structure of the PnC.

Particularly interesting are the two pronounced peaks of the PnC VDOS at 625 GHz and 750 GHz. Similar peaks are present up to frequencies of 1.4 THz. The nature of these peaks is still unclear. A possible explanation is that these are manifestations of localized modes in the nanowires.

A better understanding of the vibrational properties of the PnC system requires a knowledge of the band structure of the vibrational modes. This has been derived from calculations of the plane-wave projected VACF (Eq. 3). The function $g_{\mathbf{q}}^{\mathbf{p}}(\nu)$ was calculated for different wave vectors \mathbf{q} and the frequencies of the low lying modes were then obtained by fitting the peaks at low frequencies to Lorentzians. For the polarization vectors the x- y- and z-directions were used. This allows the separation of the out-of-plane flex modes moving along the z-direction from the in-plane modes. In-plane modes are more difficult to distinguish since, except for the lowest bands, most modes cannot be easily classified as transverse or longitudinal.

It should be noted that for the determination of the band structure, it is not sufficient to rely on the VACF determined for \mathbf{q} -vectors in the first Brillouin zone, only. In first Brillouin zone, only the lowest modes show a clear signal in the VACF. To determine the frequency of modes belonging to higher bands, one has to consider data from higher order Brillouin zones. The VACF was therefore calculated for each \mathbf{q} vector in multiple Brillouin zones and the function with the strongest signal was used to determine the mode frequency.

The band structure derived from the MD simulations is shown in Fig. 3. The figure shows the occurrence of an acoustic band gap in the longitudinal modes along the Γ -M direction. The transverse-acoustic (TA) branch along this direction has its maximum at the M point at 18 GHz. The next longitudinal mode along this direction is the first optical band starting at the Γ point at 56 GHz. If one considers the other directions shown in Fig 3, the maximum of the TA branch is at the K point close to

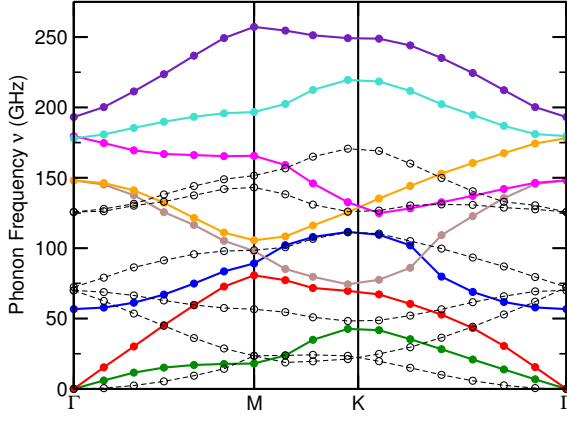


FIG. 3. (Color online) Phonon band structure obtained from the MD simulations. Circles show the calculated data points. Lines are only a guide to the eye. Full circles and solid lines show data for in-plane modes whereas open circles and dashed lines belong to out-of-plane (flex) modes.

42 GHz leaving an absolute band gap of more than 10 GHz for longitudinal modes (excluding the out-of-plane modes).

The MD simulations were complemented by a simple linear elasticity model replicating the honeycomb lattice structure of the MD model without the nanoparticles with two-dimensional slabs of a homogeneous anisotropic elastic material. For simplicity, dimensionless units were used and the mass density set to one. The following elastic constants were used: $c_{xxxx} = c_{yyyy} = 1$, $c_{xxyy} = 0.39$, $c_{xyxy} = 0.48$. All other elastic constants were set to zero. These values were chosen to replicate the ratios between the elastic constants C_{11} , C_{12} and C_{44} of Si [14]. The anisotropic elastic wave equation for this model was then discretized with the Finite Element Method (FEM) using a mesh of 8352 equilateral triangular, linear C^0 elements per unit cell [15]. Since the model is perfectly periodic, Bloch's theorem could be applied to the discretized model allowing independent computation of the vibrational eigenmodes for each wavevector \mathbf{q} .

Fig. 4 shows the band structure of the lowest bands obtained from the FEM model. Comparison with Fig. 3 shows a surprisingly good qualitative agreement between the two band structures, in particular for the lowest bands. On the other hand, there are also notable differences. The FEM model generally shows more band crossings and there is an accumulation of four bands at the Γ point close to $\nu = 0.125$. The corresponding four bands in the MD model are separated into two groups at 150 GHz and 180 GHz. Nevertheless, the qualitative agreement between the two models is evidence that the VACF method can be used to calculate band structures even for systems as large and complicated as the PnC system in this work.

In addition to the vibrational frequencies, the FEM

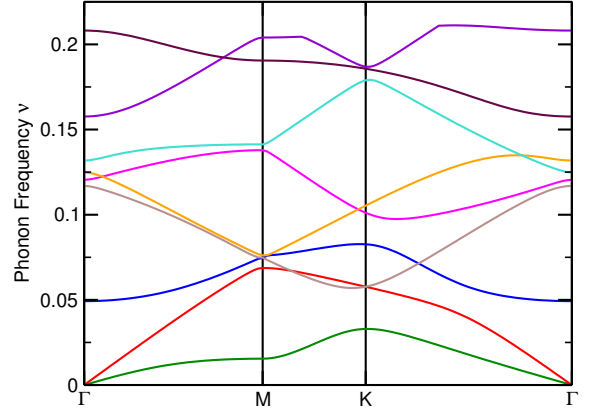


FIG. 4. (Color online) Phonon band structure obtained from the FEM model

model gives immediate access to the vibrational eigenmodes $\mathbf{u}_{\mathbf{q},\alpha}(\mathbf{r})$ where α is the band index. Fig. 5 visualizes the structure of some of the modes graphically. The left two columns show the real part of the x and y components of the vibrational modes for the wavevector at two thirds of the line from Γ to M. The imaginary parts of the solution are not shown since they look quite similar except for being shifted by half a wavelength. Instead, the columns on the right show the absolute values of the components of the solution which is proportional to the vibrational amplitude of the modes.

The left panels of modes a) and b) in Fig. 5 show that these two modes are waves vibrating in the transverse and longitudinal direction respectively. The panels on the right, however, show dark spots in the middle of the horizontal nanowires (more pronounced in the first mode). These dark spots mean that the centers of the nanowires vibrate at a lesser amplitude than the vertical zigzag chains between them. For a perfect plane wave, all areas of the system would vibrate at the same amplitude and the panels on the right would show uniform colors. This behavior is seen for all modes belonging to these bands. At long wavelength, the modes are very close to the plane wave behavior. As the wavelength gets shorter, the vibration of the modes gets more concentrated onto the zigzag chains.

The third row of Fig 5 has a very different structure. This mode clearly has its strongest amplitude at the centers of the horizontal wires which vibrate in the transverse direction whereas the right panels show that the connection points of the wires (where the nanoparticles are in the MD model) do not vibrate at all. The diagonal wires show some vibration along the x direction. The mode can therefore not be classified clearly as transverse or longitudinal with respect to the direction of the wave vector. A better classification might be given by the direction of the vibrations with respect to the axis of the nanowires. The figure shows that mode c) favors

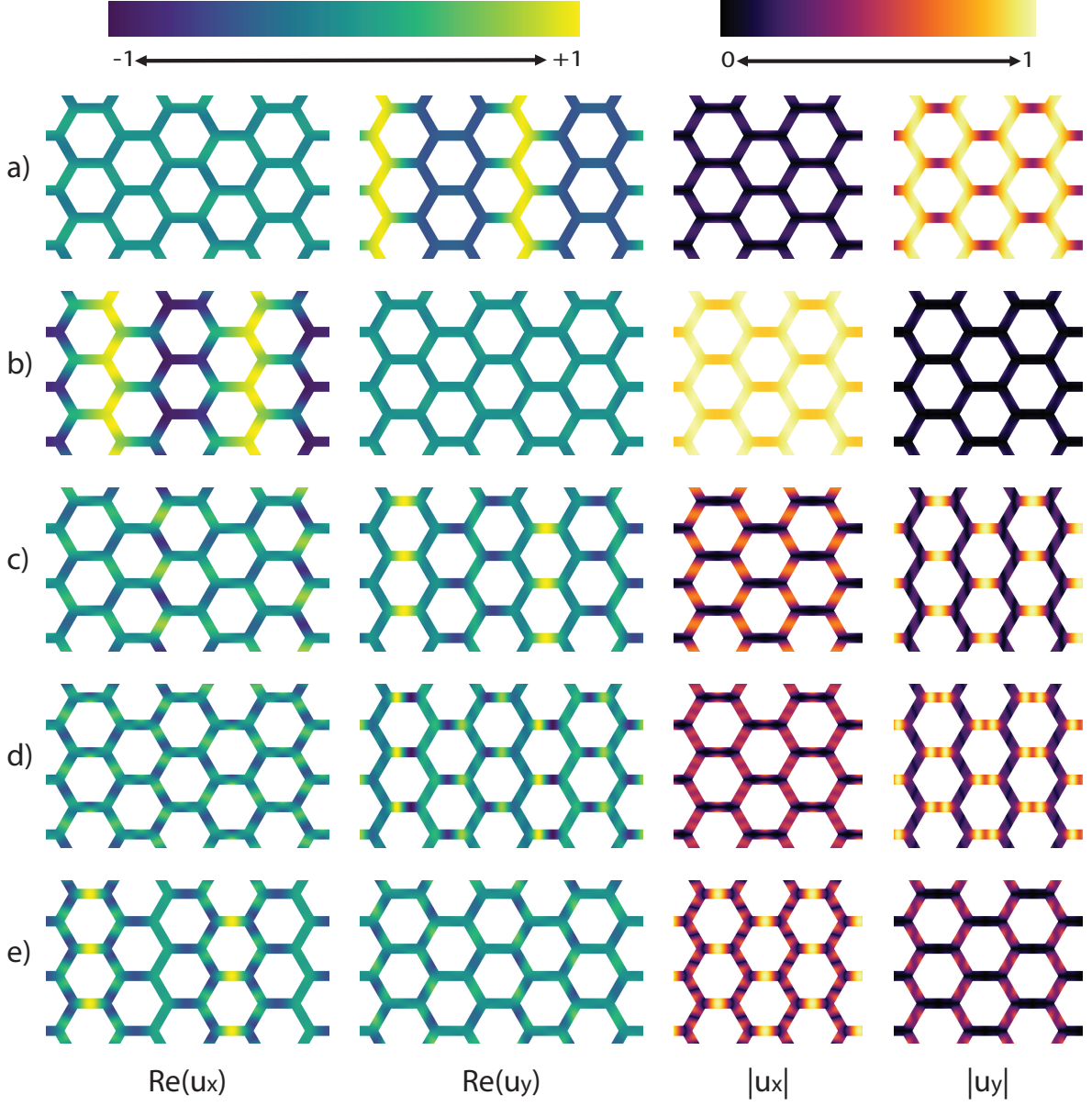


FIG. 5. (Color online) Structure of the first (a), second (b), third (c), eighth (d) and ninth (e) lowest vibrational mode of the FEM model at $\mathbf{q} = \frac{4\pi}{3\sqrt{3}a}(1, 0)$.

vibrations transverse to the wire axis.

The lowest two rows in Fig 5 show modes belonging to higher bands. Mode d) is somewhat similar to mode c), however in this case, the vibrating nanowires have two amplitude maxima and a node in the middle. Finally, mode e) is like a longitudinal counterpart to mode c). In this mode the horizontal wires vibrate along the x direction whereas the diagonal wires have some activity in the y direction. Generally the vibrations are therefore along the nanowire axis. The intersection points are again at rest. The results here indicate that the low-lying modes of the PnC can be classified according to the number of amplitude maxima along the nanowires.

In summary, the vibrational properties of a bottom-up built PnC, assembled from Si nanoparticles and nanowires, have been studied with large-scale MD simulations. The band structure derived from the simulations with the help of the VACF shows the existence of acoustic band gaps in the PnC. The general structure of the band structure is confirmed by FEM calculations of a simple two-dimensional model system. The vibrational modes obtained from the FEM model show how the vibrational modes in the PnC deviate from the plane wave behavior. For shorter wave length the vibrations of the nanowires are decoupled from the intersection points of the model and governed by separate modes.

I thank A. Serghini Mounim for helpful discussions about the application of Floquet theory infinite element calculations. This work has been supported financially by Laurentian University and the Natural Sciences and Engineering Research Council of Canada (NSERC). Generous allocation of computer time on the facilities of Compute/Calcul Canada is gratefully acknowledged.

* rmeyer@cs.laurentian.ca

- [1] P. A. Deymier, ed., *Acoustic Metamaterials and Phononic Crystals* (Springer, Berlin Heidelberg, 2013).
- [2] A. Khelif and A. Adibi, eds., *Phononic Crystals* (Springer, Heidelberg, New York, 2016).
- [3] T. Gorishnyy, C. K. Ullal, M. Maldovan, G. Fytas, and E. L. Thomas, Phys. Rev. Lett. **94**, 115501 (2005).
- [4] J.-N. Gillet, Y. Chalopin, and S. Volz, J. Heat Transfer **131**, 043206 (2009).
- [5] B. Davis and M. Hussein, AIP Adv. **1**, 041701 (2011).
- [6] D. F. Goettler, M. F. Su, C. M. Reinke, S. Alaie, P. E. Hopkins, R. H. Olsson III, I. El-Kady, and Z. C. Leseman, AIP Adv. **1**, 042001 (2011).
- [7] N. Swintek, P. A. Deymier, K. Muralidharan, and R. Erdmann, “Acoustic metamaterials and phononic crystals,” (Springer, Berlin, Heidelberg, 2013) Chap. 9.
- [8] R. Ramprasad and N. Shi, Appl. Phys. Lett. **87**, 11101 (2005).
- [9] M. I. Baskes, Phys. Rev. B **46**, 2727 (1992).
- [10] P. Heino, Eur. Phys. J. B **60**, 171 (2007).
- [11] R. Meyer and D. Comtesse, Phys. Rev. B. **83**, 014301 (2011).
- [12] R. Meyer, Phys. Rev. E **88**, 053309 (2013).
- [13] C. Z. Wang, A. Fasolino, and E. Tosatti, Phys. Rev. B **37**, 2116 (1988).
- [14] J. deLaunay, Solid State Phys. **2**, 220 (1956).
- [15] G. Dhatt and G. Touzot, *The Finite Element Method Displayed* (John Wiley & Sons, Chichester, New York, 1984).